MAUSAM, **68**, 2 (April 2017), 253-260

551.511.3 : 551.515.2 (512.317)

Observation and simulation of mountain wave trains in a tropical cyclone situation

LI Lei[#]**, P.W. CHAN* and S. M. TSE*

[#]*Shenzhen National Climate Observatory, Meteorological Bureau of Shenzhen Municipality*

**Hong Kong Observatory, 134A Nathan Road, Kowloon, Hong Kong, China*

***Shenzhen Key Laboratory of Severe Weather in South China*

(*Received 21 June 2016, Accepted 19 September 2016*)

e mail : pwchan@hko.gov.hk

सार – इस शोध पत्र में उष्णकटिबंधीय चक्रवात के समय पहाड़ों की ढलान पर तरंगावलियों का प्रेक्षण रेडार से किया गया और यहां प्रस्तुत किया गया है। तरंगावलियों से संबद्ध पवन विक्षोभ एक साथ प्रबल दक्षिण पूर्वी हवाओं के प्रवाह के परिणामस्वरूप निम्न स्तर पर पवन अपरूपण की परिघटना का रेडार द्वारा पता लगाया गया है। अतः यह विषय केवल वैज्ञानिक दृष्टिकोण से ही दिलचस्प नहीं है बल्कि इसके व्यावहारिक प्रयोग का भी महत्व है। तरंगावलियों के बनने के समय उपरि वायु आरोहण आँकड़ों से समान रूप से सूत्रपात करते हुए परिकलानात्मक तरल गतिकीय मॉडल का उपयोग करते हुए तरंगावलियों को अनुकरित किया जा सकता है। निम्न स्तर पवन अपरूपण की परिघटना के पूर्वानुमान के लिए साधारण सेट अप में ऐस मॉडल का प्रयोग करते हुए विभव की ओर संकेत करते हैं।

ABSTRACT. This paper documents the observations by radar of wave trains downstream of mountains in a tropical cyclone situation. The wind disturbances associated with the wave trains together with the background strong southeasterly flow result in the occurrence of low-level wind shear as detected by the radar. So the case is not just scientifically interesting, but it also has practical application value. The wave trains can be simulated by using a computational fluid dynamics model initialized homogeneously by the upper air ascent data at the time close to that the occurrence of the wave trains. This points to the potential of using such a model in simple setup to forecast the occurrence of low-level wind shear.

Key words – Terminal Doppler Weather Radars (TDWRs), CFD model, Wind shear, Radial velocity.

1. Introduction

Hong Kong International Airport (HKIA) is situated in an area of complex terrain. It is surrounded by seas at three sides and there is a mountainous Lantau Island to its south. There are a number of tall mountains on Lantau Island, reaching a height of about 1000 m above mean sea level (amsl). Between the mountains there are valleys having a height of about 400 m amsl.

Under favourable meteorological conditions, there are a number of terrain-disrupted airflow features occurring over HKIA as captured by the Terminal Doppler Weather Radars (TDWRs) in rainy weather and Doppler Light Detection And Ranging (LIDAR) systems in non-rainy weather condition. Such features include vortex/wave shedding (Li *et al*., 2013) and mountain waves (Chan and Hon, 2016). They have been documented and simulated using mesoscale meteorological model and its coupling with computational fluid dynamics (CFD) models in these papers. In these past cases, the terrain-disrupted airflow occurs at rather low altitudes so that they are captured by the scans with lower elevation angles by these remote-sensing meteorological instruments.

The mountain wave studies dated back to 1960s. For instance, Sarker (1966, 1967) studied the mountain waves in India and the orographically induced precipitation. More recently, theoretical study and numerical solution of the theoretical equations for mountain waves in India had been conducted by Dutta (2005), Dutta (2007a&b).

The present paper documents a case of mountain wave when Hong Kong was under the influence of strong

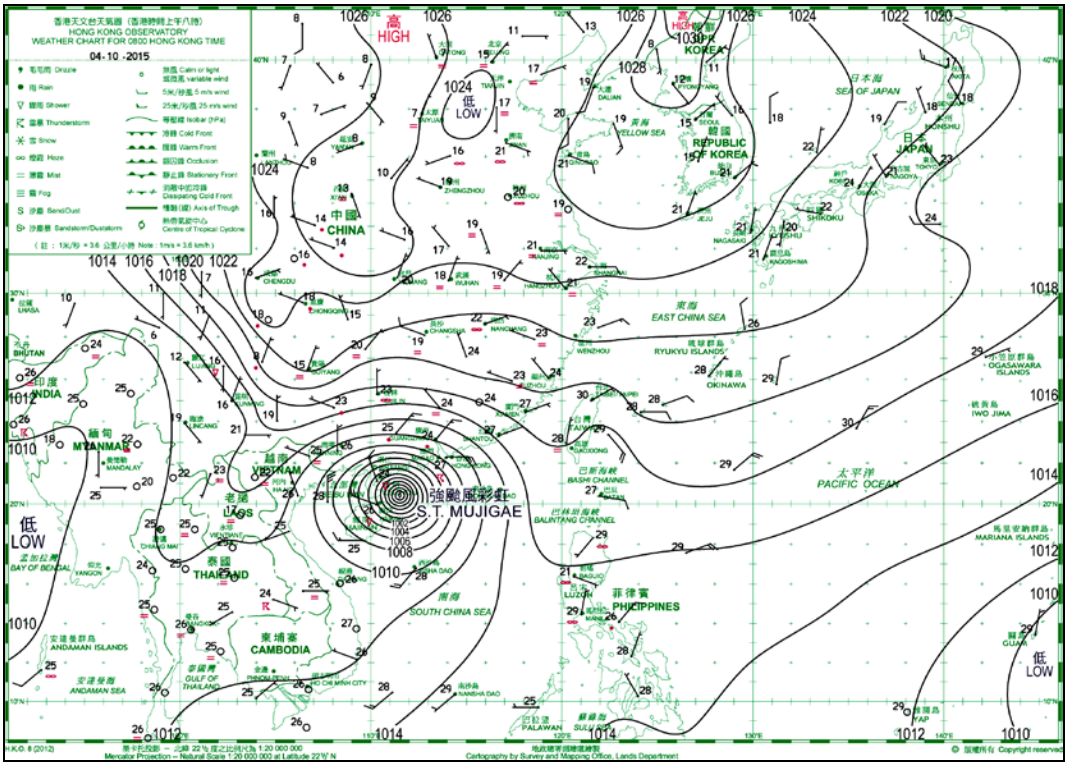

Fig. 1. Surface isobaric chart at 0000 UTC; 4 October, 2015

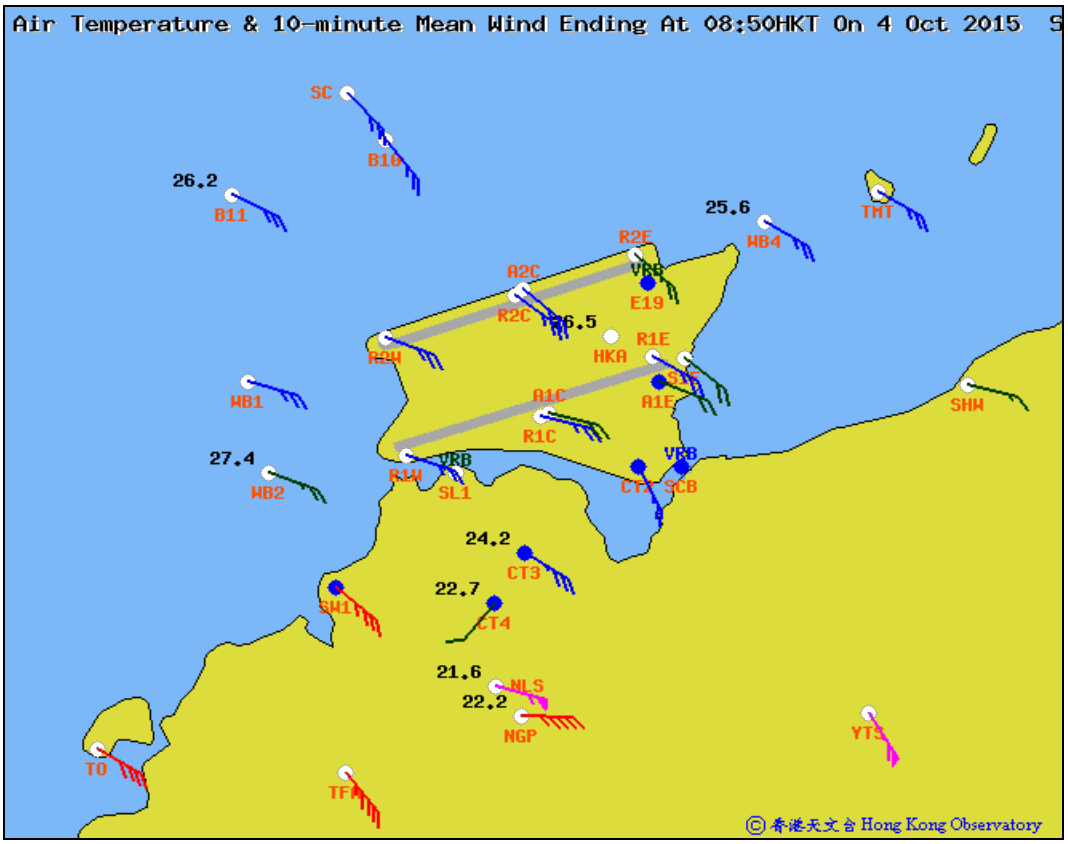

Fig. 2. Surface observations around HKIA at 08:50; 4 October, 2015 Hong Kong time (= UTC + 8 hours)

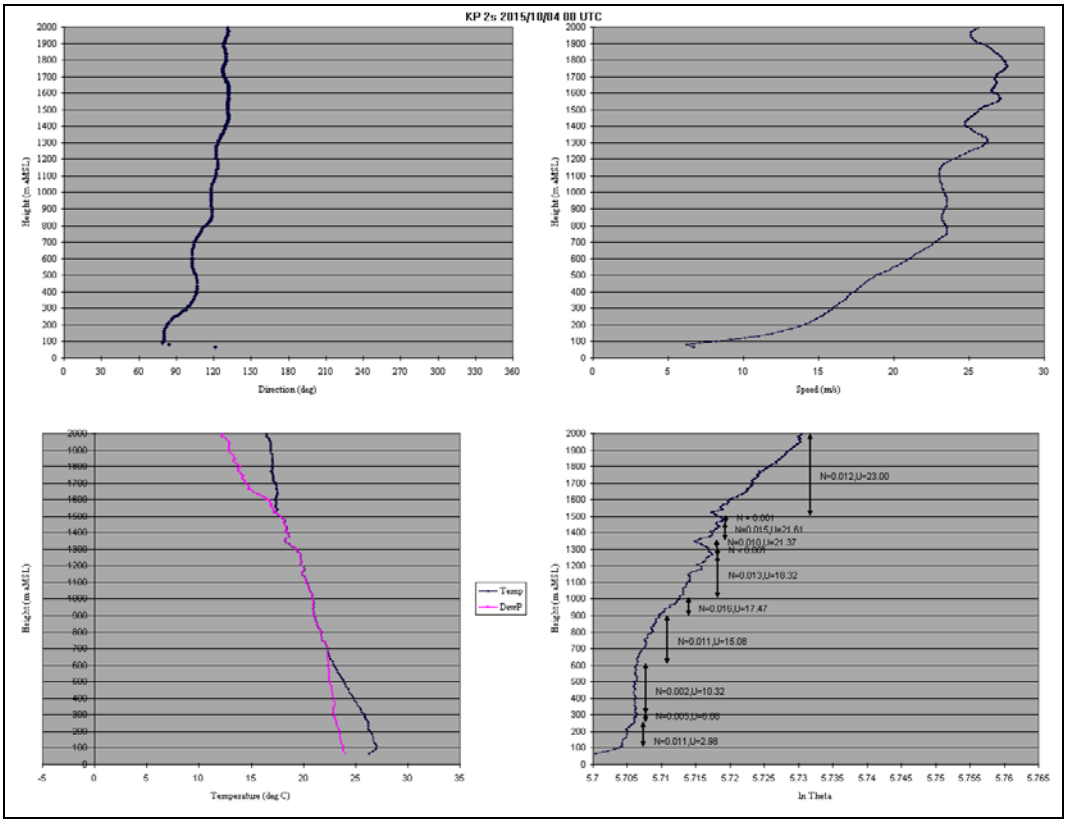

Fig. 3. Upper-air ascent data at 0000 UTC; 4 October, 2015 (upper panel: wind direction and wind speed; lower panel: temperature/dew point, potential temperature)

winds associated with a tropical cyclone. The salient features of this case include:

(*i*) The terrain-disrupted airflow occurs at higher altitudes (about 500 - 800 m amsl), so that it is captured by TDWR's conical scan at an elevation angle of 2.2 degrees;

(*ii*) The disrupted airflow brings about low-level wind shear, as determined by the wind shear detection algorithm of TDWR, so that it would be potentially hazardous to the aircraft operating at HKIA;

(*iii*) The mountain wave occurred in strong wind condition of a tropical cyclone without temperature inversion, as compared with a mountain wave in Chan and Hon (2016) when there is temperature inversion within the atmospheric boundary layer; and

(*iv*) The airflow disruption is simulated by homogeneous initialization by a CFD model, to test the capability of this relatively simple modelling setup (compared with mesoscale meteorological modelling and its coupling with a CFD model) in forecasting the occurrence of the mountain wave.

The case under study occurred when Hong Kong was under the influence of Severe Typhoon Mujigae. This typhoon tracked generally northwestwards over the northern part of the South China Sea (Fig. 1). In the morning of 4 October, 2015, when Mujigae was located at about 100 km to the southwest of Hong Kong, it brought about gale force east to southeasterly winds to HKIA. The surface wind observations near the airport by that time are given in Fig. 2. It can be seen that there was significant wind speed difference between the ground and the mountains. The winds over the airport and the adjacent islands were generally strong in force. However, it was much windier at the mountain tops and valleys, reaching about 60 knots (storm force). Under the high winds, there was frequent occurrence of low level wind shear and turbulence. There were about 75 flights reporting the encountering of low level wind shear and thus having to conduct miss approach on arrival at HKIA.

2. Observation data

The vertical profiles of the meteorological variables at 0000 UTC, 4 October, 2016 are given in Fig. 3. Relatively sharp vertical gradient of the wind speed can be seen below 700 m or so. This sharp change of the wind

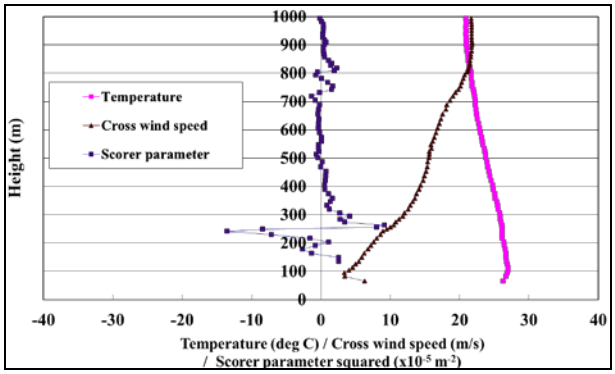

Fig. 4. The temperature, cross wind speed and Scorer parameter squared as a function of height based on the King's Park radiosonde data at 0000 UTC; 4 October, 2015

was consistent with the surface wind observations. On the other hand, wind direction did not change much in the atmospheric boundary layer. From the temperature profile, no significant temperature inversion can be identified. Parts of the atmospheric boundary layer were saturated with high relative humidity.

The occurrence of wave train is tested using the Scorer parameter based on the radiosonde data at 0000 UTC; 4 October, 2015. The Scorer parameter l is given by:

$$l^2 = \frac{N^2}{U^2} - \frac{1}{U}\frac{d^2U}{dz^2} \qquad (1)$$

where, N is the Brent-Vaisala frequency, U the magnitude of the wind component perpendicular to the mountain and z the height. The vertical variation of the Scorer parameter with height is given in Fig. 4. It could be seen that, in the range of height of interest (from about 250 m to 700 m above mean sea level), the Scorer parameter squared is generally falling this height. As such, the atmospheric condition is favourable to the occurrence of mountain wave over this range of altitudes.

TDWR is located around 12 km east-northeast of HKIA. Radial direction of radar beams generally align with runway corridor. It is a C-band radar with transmission frequency of 5.625 GHz. It generates a pencil beam with -3 dB beam width of 0.55º by an antenna of 7.9 m diameter. The transmitted pulse width is 1.0 μs. Peak transmission power of TDWR is 250 kW and the average power is 500 W. Except the antenna and antenna servo controller, all other components of TDWR are in dual configuration for redundancy. TDWR operates in two modes, monitor and hazardous modes, depending on weather. In both modes, it takes five minutes to complete a volume scan. In monitor mode when weather is not wind shear conducive, a total of 14 elevations from 0.6º to 23.0º are scanned successively. The lowest two elevations, 0.6º and 1.0º, are scanned at a slower pace of 2 rotations per minute (rpm) while other elevations are scanned at 4 rpm. In hazardous mode when there is severe weather around the HKIA, 15 elevations from 0.6º to 17.0º with the antenna moving at 4 rpm are scanned. Visiting frequency of the lowest elevation (0.6º) increases to around once every minute, *i.e.*, 5 times in a volume scan, to provide rapid update of low level wind shear and microbursts.

TDWR detects wind shear and microburst using radial velocity data of conical scans at the lowest elevation. Some descriptions of the algorithm could be found in Appendix.

3. Observational evidence and discussion

The radial velocity plots obtained by the conical scans of TDWR at an elevation angle of 2.2º are shown in Fig. 5 at two times, which occur at about 0100 UTC; 4 October, 2015. It can be seen that there is a sequence of small areas (with dimensions below 1 km) of reverse flow compared with the general wind direction in the region downstream of Lantau Peak (height of 934 m amsl) and Sunset Peak (height of 869 m amsl). The locations of these two peaks can be found in Fig. 2. Closer to the mountain, there is relatively high speed flow towards the TDWR (blue in Fig. 5) compared with the background of cross-radial flow (yellow) in the region. For distances away from the mountain, there is cross-radial flow (yellow) against the background of strong winds away from the TDWR (pink and purple). This pattern of "wave train" moves a bit with time and can be found at the two instances in Fig. 5. The wavelength is about 1.5-2 km (length scale is given in Fig. 5 by the dimensions of the square boxes to the two sides of the runways, the so-called wind shear alerting arenas).

Associated with the two wave trains, there are elongated areas of low-level wind shear (red ellipses in Fig. 5). According to the algorithm of TDWR, such wind shear is detected at 0.6º elevation conical scan over the airport area, where wave trains seem to occur downstream of Lantau Peak and Sunset Peak (not shown). However, because of the blockage of the TDWR beams by the mountains, the source of origin of such wave trains was not well shown up in this lower elevation scan. The wave trains extend to greater heights as shown in the 2.2º conical scans, and their sources appear better in such scans, namely due to terrain-disrupted airflow by Lantau Peak and Sunset Peak. They are associated with the occurrence of low-level wind shear as determined by the wind shear alerting algorithm of TDWR. As a result, the

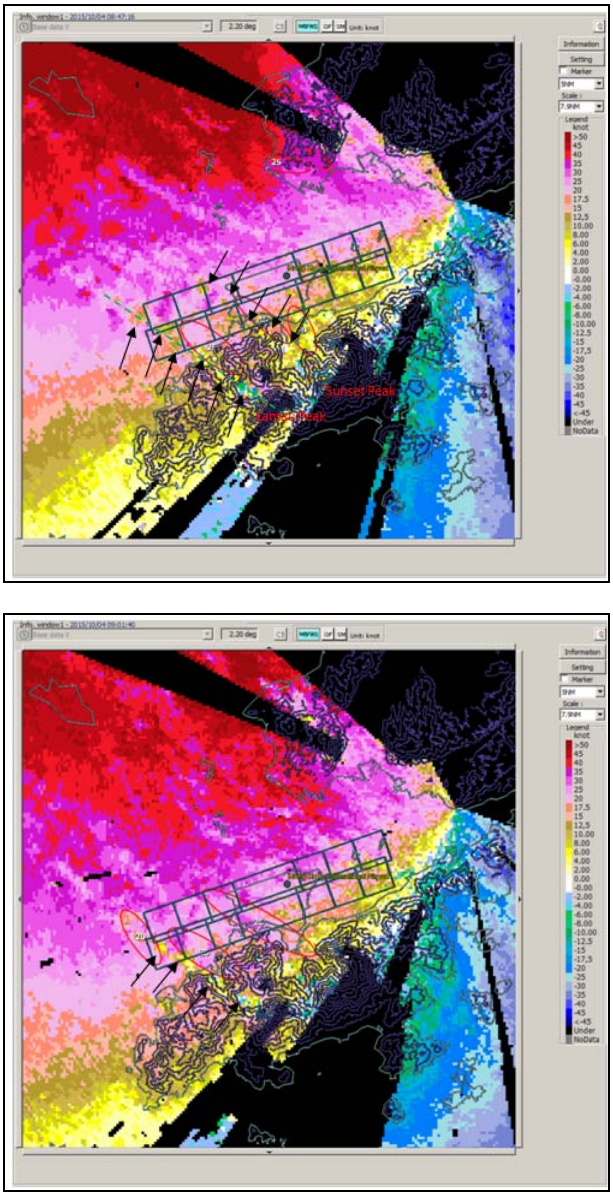

Fig. 5. TDWR radial velocity plot for 2.2º 08:47 and 09:01; 4 October, 2015 Hong Kong time. The areas of wind shear are given as ellipses with the strength of wind shear given in the headwind change magnitude (knots) as shown in the centre of the eillpses. The wave trains are indicated by arrows. The square boxes on the two sides of the runway have a length of 1 nautical mile (=1.852 km). The location of the cross-section in Fig. 6 is given by a green dotted line

wave trains are not only interesting from scientific point of view, but they have practical applications as well.

A vertical cross section is made to the wave train with the location indicated in Fig. 5. The cross section of radial velocity is shown in Fig. 6. Closer to the mountain, there are a number of velocity couplets (inbound-outbound velocity couple) as highlighted in this Figure,

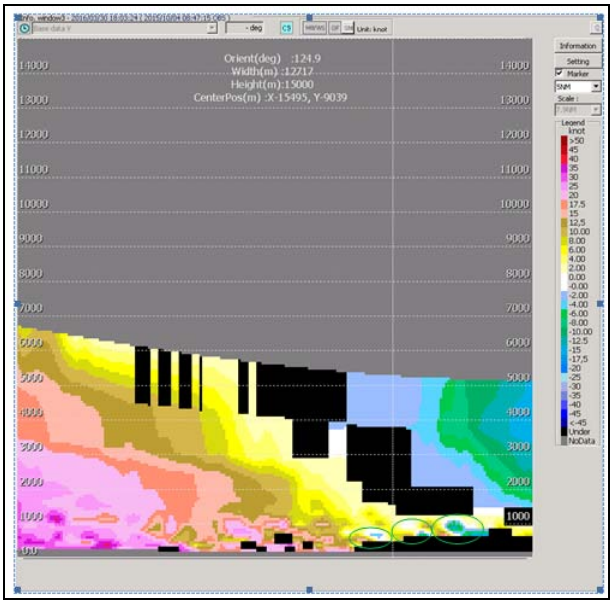

Fig. 6. Cross-section of the radial velocity at 08:47; 4 October, 2015 Hong Kong time. Velocity couplets are highlighted in green ellipses

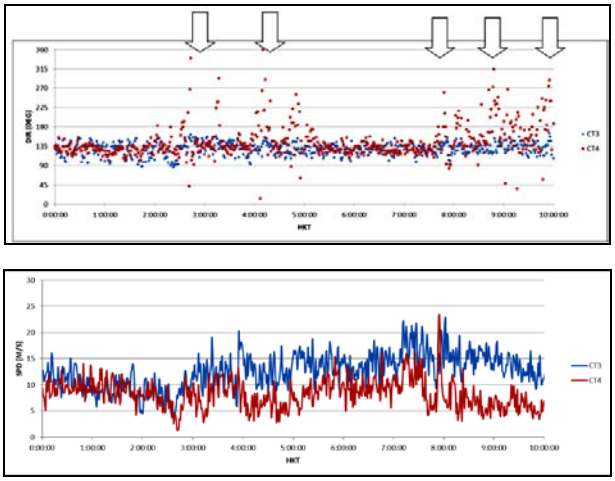

Fig. 7. The wind direction (upper panel) and the wind speed (lower panel) at the two mountain stations CT3 and CT4. The wind direction fluctuations are highlighted in arrows

and the signature is very clear. Further away from the mountain, the velocity couplet is not so apparent. Its identification becomes more difficult with the absence of some velocity data.

As a further proof of the occurrence of mountain wave, the wind speed and wind direction as recorded by the anemometers CT3 and CT4 (locations in Fig. 2) are given in Fig. 7. They have a height of about 300 and 420 m above the sea surface). It can be seen that the wind at CT3 was rather steady southeasterly. On the other hand, wind speed at CT4 was lower and there were fluctuations

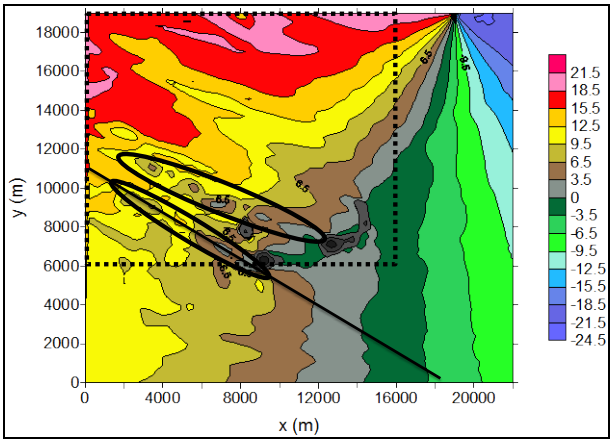

Fig. 8. Simulated radial velocity at a height of 600 m above sea surface. The wave trains are indicated by black ellipses. The zoom-in area of wind vector is given as a dotted-line rectangle

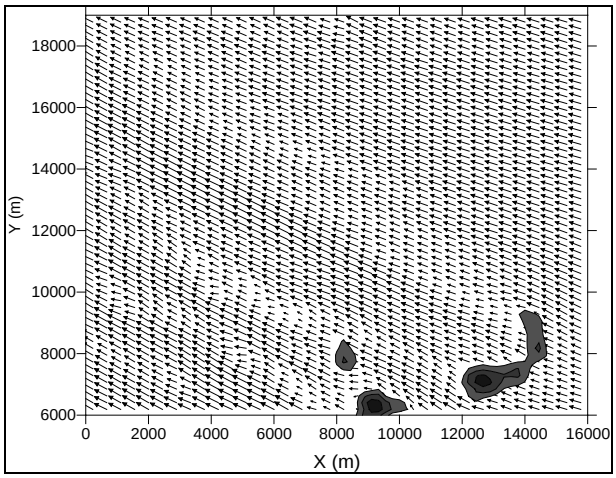

Fig. 9. The 2D wind vector for the simulation area as shown in a dotted-line rectangle of Fig. 8

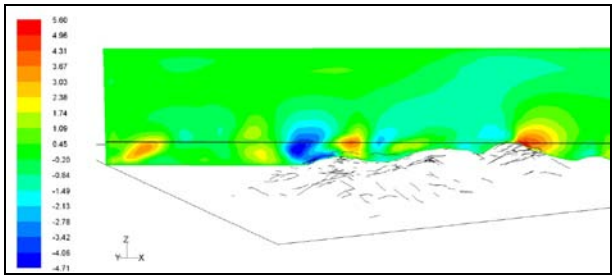

Fig. 10. Simulated w-component of the wind velocity (m/s) on the cross-section indicated by the black line in Fig. 8. The black line indicate the height of 600 m

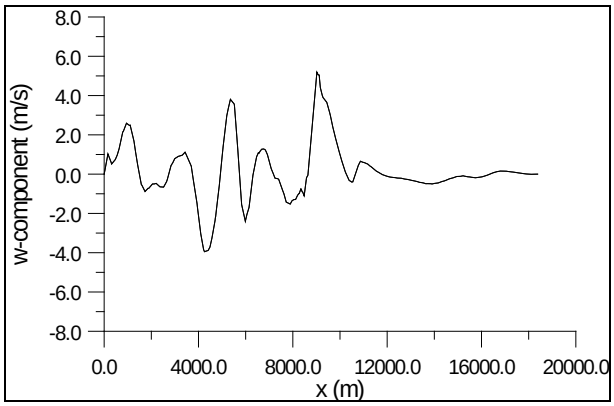

Fig. 11. Simulated w-component of the wind velocity (m/s) at the height of 600 m in the cross-section indicated by the black line in Fig. 10

in the wind direction. In Fig. 7, five fluctuations were seen, each lasting for about an hour. The fluctuations were found to be associated with the occurrence of mountain wave train.

4. CFD model

In the authors' previous studies (Li *et al*., 2013), the CFD model FLUENT was demonstrated to have capability to describe the vortex/wave shedding triggered by Lantau Island. In the current study, the domain of the FLUENT simulation has a size of 22 km × 19 km, which covers the whole airport and adjacent Lantau Island. A gridded elevation dataset is used to generate a computer-aided-design (CAD) model and a body-fitted hexahedral grid system. The cell numbers on *x* and *y* axes are 140 and 120 respectively which means the horizontal grid spaces are around 158 m in both directions. On the vertical direction, the domain reaches a height of 3000 m and is divided into 22 layers. The vertical grid space increases with a stretch ratio of 1.1 from the bottom to the top and the lowest vertical grid space is about 45 m.

The radiosonde data from King's Park weather station is used to drive the simulation, which is about 20 km to the east of HKIA. Wind and potential temperature data (Fig. 3) are converted into a text file in a predefined user-defined function (UDF) format from the original radiosonde data file. The UDF formatted file is read into FLUENT and used to drive the simulation run through boundary conditions.

A two-step method is applied in the FLUENT simulation. First, a steady simulation is performed in the Reynolds-Averaged Navier Stokes (RANS) framework, and the realizable k-ε turbulence scheme (Shih *et al*., 1995) is adopted. The results of the steady simulation are taken as the initial value of the simulation for the second step, in which an unsteady simulation in the Large-Eddy Simulation (LES) framework is performed to capture the temporal evolution of the flow field. The Smagorinsky-Lilly scheme (Smagorinsky, 1963; Lilly, 1966) is applied

as the subgrid-scale model of LES. Since the wind was quite strong in the period of simulation, the thermal process is not considered in the current simulation.

All boundaries except the bottom and north boundary of the simulation domain are set as velocity inlets. For the bottom, a non-slip boundary condition is used and the surface roughness is set at 0.0005 m for the sea, 0.005 m for the airport and 0.5 m for mountains of the island.

5. CFD solution method

In order to get a convergent solution, the SIMPLE algorithm is applied in the numerical simulation of the steady simulation with the first order upwind method applied in the discretization of momentum and turbulent variables. For the unsteady simulation, the SIMPLE algorithm is also used except for that the bounded central differencing method is used in the discretization of momentum. The commercial software FLUENT is used to realize the numerical simulation.

6. CFD modelling results and discussion

The model-simulated winds are resolved along the radials of the TDWR for easier comparison with the actual TDWR observations. The simulated radial velocity picture at a typical time is given in Fig. 8. Though the radial wind speeds are not exactly the same as the actual observations, wave trains are successfully simulated downstream of a couple of mountains on Lantau Island. The two-dimensional wind field at this time is given in Fig. 9. The wave train as simulated in the radial velocity plot is indeed a series of waves downstream of the mountains. The wavelength is in the order of 1.5-2 km, consistent with the TDWR observations. It is interesting to note that the homogeneous initialization of the CFD model using the radiosonde ascent (Fig. 3) at 0000 UTC; 4 October, 2015 is able to reproduce the TDWR-observed mountain wave feature.

In order to study the wavy structure in the numerical simulation with more details, a cross section to the flow field is made at the location at shown in Fig. 8. Fig. 10 shows the vertical velocity distribution on this cross section. It can be seen that there are variations of vertical velocity along this plane as a result of the airflow passing over the mountain. The positive and negative values of vertical velocity (corresponding to upward and downward motion) appear alternately. A horizontal line is drawn as a black line along the cross section in Fig. 10. And the numerical value of the vertical velocity along this line is given in Fig. 11. This has a height of 600 m above the sea surface. It serves as a demonstration of the variation of the vertical velocity along this line, and the mountain wave is clearly shown here.

TABLE 1

Comparison of the observed & the simulated mountain wave trains

Element	Observed	Simulated
Wavelength	About 2 km	About 2.5 km
Height range over which waves occur	Between about 400 m and 900 m above the sea surface	Between about 300 m and 1000 m above the sea surface
Distance from the mountain over which waves occur (from the mountain uptill that point that the waves are hardly discern able	About 10 km	About 9 km

Some characteristics of the observed and the simulated waves are compared in Table 1. It could be seen that the simulation could successfully reproduce some key features of the observed waves.

7. Conclusion

A case of wave train downstream of mountains in tropical cyclone situation is documented in this paper. The wave train also leads to the occurrence of low-level wind shear as detected by radar. Its occurrence is well simulated with a CFD model with homogeneous initialization with the upper-air ascent data at a given time. The wave train is scientifically interesting on its own right, but it also has application in the day-to-day meteorological service. In fact, the Typhoon Mujigae case has led to historically the largest number of miss approach of landing aircraft in a tropical cyclone situation at HKIA due to wind shear. The wind shear events are studied in detail and the results would be reported in a future paper.

Acknowledgements

This study is supported by the National Natural Science Foundation of China (Grant No. 41575005).

References

Adaeda, K., 2001, "Accuracy of wind measurements and performance of low altitude wind shear detection by terminal Doppler weather radar", *Information on Radar Observation Technology*, **49**, 10-22 (in Japanese).

Chan, P. W. and Hon, K. K., 2016, "Performance of super high resolution numerical weather prediction model in forecasting terrain-disrupted airflow at the Hong Kong International Airport: case studies", *Meteorological Applications*, **23**, 101-114.

Dutta, S., 2005, "Effect of static stability on the pattern of three-dimensional baroclinic lee wave across a meso scale elliptical barrier", *Meteorology and Atmospheric Physics*, **90**, 139-152

Dutta, S., 2007a, "A meso-scale three-dimensional dynamical model of orographic rainfall", *Meteorology and Atmospheric Physics*, **95**, 1-14

Dutta, S., 2007b, "Parameterization of momentum flux and energy flux associated with orographically excited internal gravity waves in a baroclinic background flow, *Mausam*, **58**, 459-470

Fukao, S. and Hamazu, K., 2014, "Radar for meteorological and atmospheric observations", Springer, Japan.

Hamazu, K., Ishihara, M., Hata, K., Hashiguchi, H. and Fukao, S., 2000, "Development of low-level wind shear detection algorithm for the DRAW", *Institute of Electronics, Information and Communication Engineering (IEICE) of Japan*, **7**, 1067-1080, (in Japanese).

Lei, L. I., Chan, P. W., Zhang, Li-Jie and Hui, Mao, 2013, "Numerical simulation of terrain-induced vortex/wave shedding at the Hong Kong International Airport", *Meteorologische Zeitschrift*, **22**, 317-327.

Lilly, D. K., 1966, "The representation of small-scale turbulence in numerical simulation experiments", Proceedings, IBM Scientific Computing Symposium on Environmental Sciences, November 14-16, 1966, Thomas J. Watson Research Center, Yorktown Heights, N. Y. Y., edited by H. H. Goldstein, IBM Form No.320-1951, 195-210.

Sarker, R. P., 1966, "A dynamical model of orographic rainfall", *Monthly Weather Review*, **94**, 555-572.

Sarker, R. P., 1967, "Some modifications in a dynamical model of orographic rainfall", *Monthly Weather Review*, **95**, 673-684.

Shih, T. H., Liou, W. W., Shabbir, A., Yang, Z. G. and Zhu, J., 1995, "A new k-ε eddy viscosity model for high reynolds number turbulent flows", *Computers & Fluids*, **24**, 3, 227-238

Smagorinsky, J., 1963, "General circulation experiments with the primitive equations", *Mon. Wea. Rev.*, **91**, 99-164.

Appendix

Descriptions of the TDWR wind shear detection algorithm

The detection algorithm involves the following processes based on data in polar coordinates. First, it looks for divergence segments with monotonic increasing velocity along each radial beam (Fukao and Hamazu, 2014). Only divergence segments longer than a pre-defined value are kept for the next step (Hamazu *et al*., 2000). The divergence segments are grouped into clusters, which are called features, according to overlapping distance for segments in different radials and proximity of azimuth angle of the segments. Characteristics of a feature, such as number of divergence segments, maximum velocity difference, and size etc are checked (Hamazu *et al*., 2000). If the feature can meet all pre-defined requirements, it is considered as a potential feature. The potential features are then checked with other identified features in previous two scans. If the potential feature can correlate with any features which appear in one of the previous two scans, it is considered as a valid wind shear or microburst feature (Adaeda, 2001).